Microglia Control Escalation of Drinking in Alcohol Dependent Mice: Genomic and Synaptic Drivers

Supplement 1

Table of Contents:

Supplemental Methods

Chronic Intermittent Ethanol Two-Bottle Choice Procedure

We used the chronic intermittent ethanol vapor two-bottle choice (CIE-2BC) model to produce escalated ethanol intake in dependent mice (1-3). Two cohorts of male C57BL/6J mice (Jackson Laboratory, Bar Harbor, ME) were prepared: **Cohort 1**, used for immunohistochemistry (IHC) studies, consisted of alcohol dependent (Dep), non-dependent (Non-Dep) and alcohol naïve (Naïve) mice (4 mice per group). **Cohort 2**, (used for alcohol drinking, anxiety-like testing, IHC, RNA sequencing and electrophysiological studies) consisted of 12 mice per group: alcohol-dependent mice receiving the control diet (Control Diet/Dep), alcohol-dependent mice receiving the MG depletion diet (MG Depletion/Dep), non-dependent mice receiving the control diet (Control Diet/Non-Dep) and non-dependent mice on the MG depletion diet (MG Depletion/Non-Dep).

Mice were exposed to a limited-access ethanol (15% w/v) two-bottle choice (2BC) paradigm followed by either CIE exposure in vapor chambers (La Jolla Alcohol Research, La Jolla, CA) to induce alcohol dependence or air exposure in identical chambers. To establish baseline drinking, we performed 2BC testing 5 days per week for 3 consecutive weeks (see **Figure S2**). Mice were singly housed 30min before the lights were turned off and given 2 h-access to two drinking tubes containing either 15% ethanol or water. Following this 3-week baseline phase, mice were divided into two balanced groups with equal ethanol and water consumption. The Dep and Non-Dep groups were exposed to CIE vapor and air, respectively. Mice in the Dep group were injected i.p. with 1.75g/kg ethanol + 68.1mg/kg pyrazole (alcohol dehydrogenase

inhibitor) and placed in vapor chambers for 4 days (16h vapor on, 8h off). Naïve and Non-Dep mice were injected with 68.1mg/kg pyrazole in saline. After pyrazole injection, Naïve mice were placed back in their home cages, while Non-Dep mice were transferred into air chambers for the same intermittent period as the Dep group. The vapor/air exposure was followed by 72h of abstinence and 5 days of 2BC testing. This regimen was repeated three additional times for a total of four full rounds. On the third or fourth day of vapor exposure, tail blood was collected to determine blood alcohol levels (4). Ethanol drip rates in the vapor chambers were adjusted such that BALs progressively increased over the vapor exposure rounds to a final target of 150–200 mg/dL.

Novelty Suppressed Feeding Test

Five days following the final 2BC session, mice were food-deprived for 24h. Just before testing, mice were transferred to new, clean holding cages. Testing consisted of two consecutive phases: feeding in the novel open field and feeding in the familiar home cage. The experimental arena consisted of a brightly lit (400 lux) white open field (50x 50x22-cm) lined with 2cm of fresh bedding. One fresh food pellet was placed in the center of the arena. The test mouse was placed in a corner of the arena and the latency to eat the food pellet was recorded, with a cutoff time of 10min. The mouse was removed as soon as it began eating and was immediately transferred to its home cage with a single food pellet. The latency to begin to eat this pellet was recorded, with a cutoff time of 5min. The mouse was then returned to its home cage with free access to food and water.

Immunohistochemistry

Mice (n=23) were anesthetized using isoflurane and perfused transcardially with cold phosphate-buffered saline (PBS)/Z-fix (Fisher Scientific, Waltham, MA). Brains were dissected and immersion fixed in Z-fix for 24h at 4°C, cryoprotected in sterile 30% sucrose in PBS for 24-48h at 4° C, flash frozen in pre-chilled isopentane on dry ice and stored at -80°C. Brains were then sliced on a cryostat in 35 µm thick sections and free-floating sections were stored in cryoprotective solution (50% v/v phosphate buffer, 30% w/v sucrose, 1% w/v polyvinylpyrrolidone, 30% v/v ethylene glycol) at −20°C until use.

Chromogenic Immunohistochemistry

Free-floating brain sections were rinsed with PBS, and endogenous alkaline phosphatase was quenched with BLOXALL (Vector Laboratories, Burlingame, CA) for 20 min. Sections were blocked in 5% normal donkey serum, 0.3% Triton-X100 and 1 mg/ml BSA for 1h followed by overnight incubation at 4°C in rabbit anti-IBA1 (Ionized Calcium-Binding Adapter Molecule 1) (1:1000, 019-19741; Wako Chemicals USA, Richmond, VA) diluted in PBS with 0.5% Triton X-100 (PBS-TX) plus 2% normal donkey serum. After a PBS wash, IBA1 staining was visualized using the ImmPRESS™-AP Anti-Rabbit IgG (alkaline phosphatase) Polymer Detection and ImmPACT Vector Red Substrate Kits (Vector Laboratories, Burlingame, CA). All sections were washed in PBS between steps and after substrate reaction. Sections were mounted onto Superfrost Plus (Thermo Fisher Scientific, Waltham, MA) slides, dried overnight, dehydrated in increasing concentrations of ethanol and permanently mounted with DPX (Thermo Fisher Scientific, Waltham, MA). The central nucleus of the amygdala (CeA)

(lateral/medial) and medial prefrontal cortex (mPFC) (infralimbic/prelimbic) were imaged with a Leica SCN400 scanner (Leica Microsystems, Buffalo Grove, IL). Identical settings were used for image analysis within experiments. Analyses were conducted using Image Pro Premiere (Media Cybernetics, Inc., Rockville, MD). Raw-integrated optical density and cell counts in the CeA and mPFC were measured. Brightness/contrast were the same for all representative images shown.

Fluorescent Immunohistochemistry

Brain sections were blocked in 10% normal donkey serum in PBS for 2h at room temperature followed by incubation overnight at 4^{o}C in a primary antibody cocktail containing goat anti-IBA1 (1:500, ab5076, Abcam, Cambridge, MA) and monoclonal rabbit anti-TMEM119 (5) (Transmembrane Protein 119) (1:500, ab209064, Abcam) diluted in PBS with PBS-TX plus 2% normal donkey serum. The following day, sections underwent three washes of 5min each in PBS-TX and were then incubated for 2h at room temperature in Alexa Fluor 647-conjugated donkey anti-goat (1:500, 705-605-147, Jackson Immunoresearch, West Grove, PA) and Alexa Fluor 488-conjugated Donkey anti-rabbit (1:500, 711-545-152, Jackson Immunoresearch) in PBS-TX with 2% normal donkey serum. Sections were subsequently washed in PBS-TX and then incubated for 1 h in Hoechst 33342 in PBS (1:1000, H3570, Life Technologies, Carlsbad, CA). Lastly, sections were washed in PBS and deionized water and then mounted onto Superfrost Plus (Thermo Fisher, Waltham, MA) slides using ProLong Gold Antifade Mountant (P10144, Thermo Fisher). Antibodies were validated by omission of primary antibody. The IBA1 antibody has been used extensively for IHC in mouse tissue (6) and is

blocked by pre-adsorption with the corresponding antigen (7). Development and specificity of the TMEM119 antibody have been thoroughly described (5). Slides were imaged on a Zeiss LSM 780 laser scanning confocal microscope (40X oil immersion, 1024x1024, 10-µm z-stacks) in the mPFC (infralimbic/prelimbic) and CeA (medial). Identical microscope settings were used for image acquisition within experiments. ImageJ (8) was used to count DAPI-stained nuclei labeled with the fluorescent probe of interest. For each probe, the signal intensity present after background subtraction identified the positive nuclei. The experimenter was blind to the treatment group during quantification. Analyses and statistics were performed using R programming (9). Significance was determined by two-way ANOVA. Brightness/contrast were the same for all representative images shown.

RNA-Sequencing

The mPFC was freshly dissected, flash frozen and stored in RNAse-free 1.5 mL tubes. The remaining section of brain was flash frozen and embedded in plastic molds containing optimal cutting temperature medium. 300µm sections were cut on a Microm HM550 Cryostat. Micropunches containing the CeA were punched using a 0.75mm punch (Stoelting, WoodDale, IL). Total RNA was isolated using the MagMAX-96 Total RNA Isolation Kit (Life Technologies, Grand Island, NY). Total RNA was quantified using a NanoDrop 8000 spectrophotometer (Life Technologies) and assessed for quality using the 2200 Agilent TapeStation (G2965AA, Agilent Technologies, Santa Clara, CA). Contaminating DNA was removed using a DNA-free Kit (Thermo Fisher Scientific). Only samples with RNA integrity number (RIN) values > 7 were used in the

analysis. Sample RNA concentrations for RNA-sequencing ranged from 23-558ng/µl, with RIN scores ranging from 7.1–8.7. Group sample sizes for the mPFC were as follows: (1) Control Diet/Dep, n=9; (2) MG Depletion/Dep, n=9; (3) Control Diet/Non-Dep, n=7; (4) MG Depletion/Non-Dep, n=9. Group sample sizes for the CeA were as follows: (1) Control Diet/Dep, n=5; (2) MG Depletion/Dep, n=4; (3) Control Diet/Non-Dep, n=6; (4) MG Depletion/Non-Dep, n=4.

A minimum of 1 ng RNA per sample from the mPFC and CeA was submitted to the Genomic Sequencing and Analysis Facility at the University of Texas at Austin for 3'UTR transcriptome sequencing. Sequencing libraries were constructed using a 3' Tag-based approach (TagSeq), targeting the 3' end of RNA fragments from ~80ng/uL of each RNA sample (10). This tag-based approach is a cost-efficient alternative to whole-transcriptome RNA sequencing, comparable with respect to accuracy and quantification of detected transcripts (10). mPFC samples were pooled, size selected with Pippin Prep (Sage Science, Beverly, MA) then sequenced on a Single End Run using the HiSeq 2500 (Illumina Inc., San Diego, CA) to a read depth of ~4 million reads per sample (10). CeA samples were then pooled, size selected with Pippin and sequenced on a Single End Run using the NovaSeq 6000 (Illumina Inc.) to a read depth of ~4 million reads per sample (10). Both mPFC and CeA sequencing runs were spiked with External RNA Controls Consortium (ERCC; Thermo Fisher Scientific) to validate the dynamic range for our sequencing depth (11).

Bioinformatics

Reads were mapped to the mouse reference genome (UCSC, mm10) using the alignment tool Bowtie2 (v2.3.4.3). Raw RNA-sequencing files were evaluated for quality control using FastQC (0.11.8). HTSeq (v.0.11.0) was used for counting mapped sequencing reads. Quantified read counts were normalized and analyzed using DESeq2 (v 1.10.1) to determine differential expression between groups (Control Diet/Dep; Control Diet/Non-Dep; MG Depletion/Dep; MG Depletion/Non-Dep), within the R statistical computing environment (v3.5.1). Pairwise differential expression analysis and ANOVA differential expression analysis were performed with DESeq2. Identical read filtering parameters were used for both brain regions, and genes with read counts < 5 in at least half of the samples per treatment group were removed. Based on these parameters, we identified >13,000 genes per sample per brain region. Differentially expressed genes in the mPFC and CeA after microglia depletion and alcohol dependence are shown in Supplemental Tables 1 and 2, respectively. Genes with a nominal significance threshold of $P<0.05$ were used for further analysis. This threshold was selected to balance type-1 and type-2 error rates when performing pathway and network analyses. Normalized read counts, scaled according to the library size of individual samples.

Weighted gene co-expression network analysis (WGCNA), using filtered log2 transformed expression data, was then applied to construct scale-free networks that specify coordinately regulated genes (i.e., modules) (12). To explore the modular structures of the co-expression network, the adjacency matrix (A network adjacency matrix that is a symmetric matrix whose entries lie between 0 and 1. It is a special case

of a similarity matrix that is transformed into a topological overlap matrix (12). Because topological overlap between two genes reflects both their direct and indirect interactions with all other genes in the network, this approach helps create more cohesive and biologically meaningful data interpretation. WGCNA parameters were according to those previously used in our laboratory (13), including a minimum module size equal to 100 genes and a 0.99 tree-cut height. The maximal statistical significance for gene set enrichment was determined using a Fishers-exact test, corrected for multiple comparisons using a Benjamini-Hochberg false discovery rate (FDR)$\leq$0.05. Each module was assigned a unique, arbitrary color. Individual gene sets from modules and differentially expressed genes were functionally annotated for biological processes and pathway enrichment using the web-based software application Webgestalt (14) and Enrichr (15) and selected if they passed an adjusted P-value of P<0.05. For Webgestalt enrichment the reference gene set was the protein coding genome and at least 10 genes had to be enriched in a category or pathway in order for it to pass significance. Enrichment of gene ontologies (GOs), cell types, and DEGs in modules was assessed using Fisher's exact test corrected for multiple testing (Benjamini-Hochberg FDR$\leq$0.05). Select gene sets, based upon statistical and biological significance, were assembled to visualize network properties using the bioinformatics tool Cytoscape (v3.6.1) (16). To assess cell-type specificity, we curated lists of genes with higher expression in one cell type than all other cell types using brain-based RNA expression data (17) (http://web.stanford.edu/group/barres_lab/brain_rnaseq.html) and used Fisher’s exact test corrected for the number of modules and cell types to determine significance of enrichment.

Rank Rank Hypergeometric Overlap (RRHO) analysis was used to identify the overlap of differentially expressed gene lists between the mPFC and CeA (18-20). RRHO identifies the degree and significance of overlap between expression profiles in a threshold-free manner (18). Full differential expression lists were ranked by the -log10(p-value) multiplied by the sign of the fold change from the DESeq2 analysis. RRHO difference maps were produced for group comparisons (e.g., MG Depletion vs. Control Diet) by calculating the normal approximation of difference in log odds ratio and standard error of overlap per pixel between the groups. This Z-score was then converted to a P-value and corrected for multiple comparisons across pixels.

Electrophysiology

Mice (n=5 per experimental group) were anesthetized using 3-5% isoflurane, decapitated and their rapidly isolated brains placed in oxygenated (95% O_2/5% CO_2), ice-cold high-sucrose solution (pH=7.3-7.4) containing in mM: 206.0 sucrose; 2.5 KCl; 0.5 $CaCl_2$; 7.0 $MgCl_2$; 1.2 NaH_2PO_4; 26.0 $NaHCO_3$; 5.0 glucose; and 5.0 HEPES, as previously described (21, 22).

Brain slices (300 μm) were cut using a Leica VT1200 S vibratome (Buffalo Grove, IL) and incubated in oxygenated artificial cerebrospinal fluid (aCSF) containing in mM: 130.0 NaCl; 3.5 KCl; 2.0 $CaCl_2$; 1.25 NaH_2PO_4; 1.5 $MgSO_4$; 24.0 $NaHCO_3$; and 10.0 glucose at 37°C for 30min and then at room temperature for a minimum of 30min. Neurons in the medial subdivision of the CeA were visualized with infrared differential interference contrast (IR-DIC) optics, using either 40x or 60x water immersion objectives (Olympus BX51WI, Tokyo, Japan) and CCD cameras (EXi Aqua, QImaging,

Surrey, BC, Canada). Whole-cell voltage-clamp recordings were performed in a total of 279 neurons (186 for $GABA_A$ receptor-mediated currents and 93 for glutamate receptor-mediated currents) using gap-free acquisition mode (20kHz sampling rate/signal and 10kHz low-pass filter) with a Multiclamp 700B amplifier (Digidata 1440A) and pClamp 10 software (Molecular Devices, Sunnyvale, CA).

Spontaneous inhibitory postsynaptic currents (sIPSCs) were recorded using a KCl-based internal solution (containing in mM: 135 KCl; 5 EGTA; 2 MgCl2; 10 HEPES; 2 Na-ATP; and 0.2 Na-GTP), and pharmacologically isolated using 20μM 6,7-dinitroquinoxaline-2,3-dione (DNQX), 30M DL-2-amino-5-phosphonovalerate (AP-5) and 1μM CGP 55845A. Spontaneous excitatory postsynaptic currents (sEPSCs) were recorded using a K-gluconate-based internal solution (containing in mM: 145 K-gluconate; 0.5 EGTA; 2 MgCl2; 10 HEPES; 2 Na-ATP; and 0.2 Na-GTP), and pharmacologically isolated using 30μM bicuculline and 1μM CGP 55845A. Neurons were clamped at -60mV, and series resistance was monitored throughout the experiment using 10mV pulses. Recordings with access resistance >15MΩ or >20% change were excluded from the final data set. Brain slice recordings were performed in alcohol-free solutions under conditions of acute *in vitro* withdrawal (1-8h). E/IPSC parameters (frequency, amplitude, rise and decay times) were analyzed using Mini Analysis (Synaptosoft Inc., Fort Lee, NJ) and visually confirmed. Events <5pA were excluded from the analysis, and the average from a minimum of 60 events or a 3min interval was calculated.

Neuronal membrane properties and excitability were evaluated from voltage traces recorded in current-clamp mode. The Current-Voltage (I-V) acquisition protocol

consisted of a series of depolarizing and hyperpolarizing current steps (Δ10pA/600 ms). Recordings were performed using a K-gluconate-based internal solution (described above). Data were analyzed using the NeuroExpress software (version 19.4.09) developed and provided by Dr. A. Szücs. The membrane time constant was calculated as an average determined from monoexponential fits of the initial parts of individual voltage responses evoked by negative current steps in current clamp mode. The Voltage Sag and afterdepolarization values were plotted against the level of the injected current and the corresponding relationships were fitted with linear functions. Using Prism 8.01 (GraphPad, San Diego, CA), data were analyzed for statistical significance by two-way ANOVA and Sidak's multiple comparisons *post hoc* test.

Supplemental Figures

Figure S1

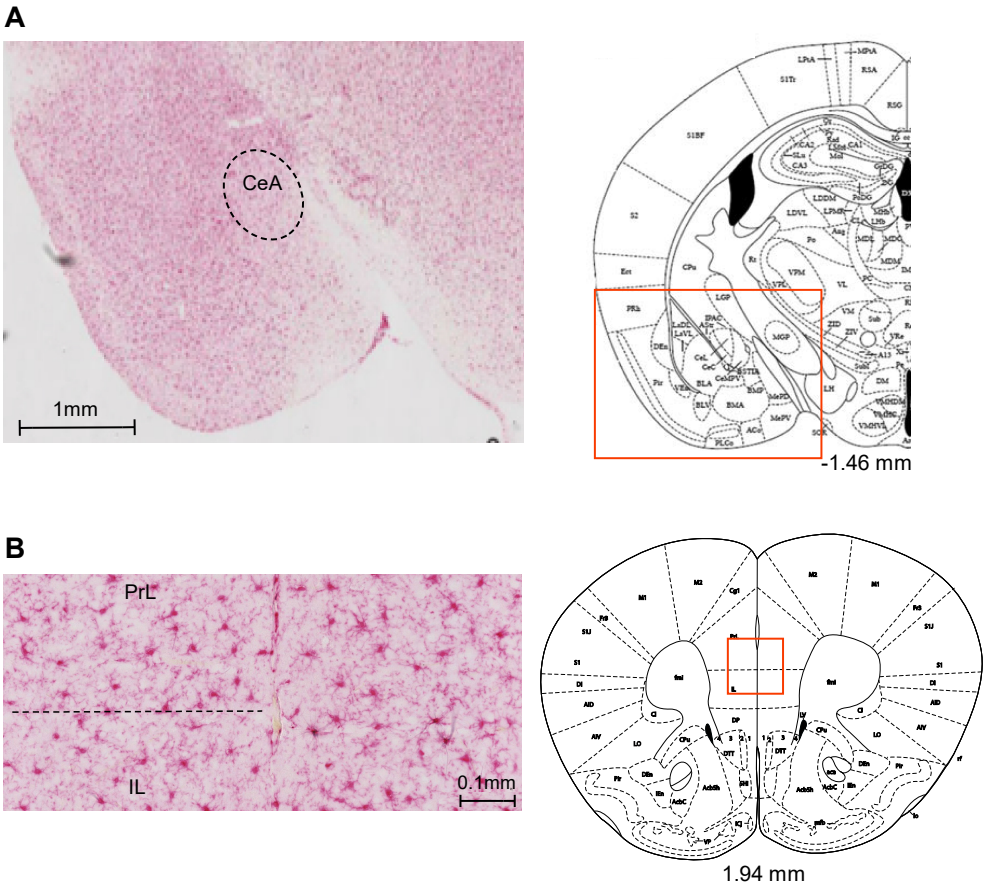

Figure S1. Representative brain slices indicating CeA and mPFC region of interest. (a) Representative amygdala image (20X) of Ionized Calcium Binding Adaptor Molecule 1 (IBA1)-labeled (red) microglia in Naïve mouse. The central nucleus of the amygdala (CeA) is indicated by the circled region of interest (ROI) on the image (left), and image acquisition position is indicated by the red box on the diagram to the right (Franklin and Paxinos, 2008) by the red box. (b) Representative medial prefrontal cortex (mPFC) image (20X) of IBA1-labeled (red) microglia. Prelimbic (PrL) and infralimbic (IL) regions are indicated on the image by the dotted line (left), and image acquisition position is indicated by the red box on the diagram to the right (Franklin and Paxinos, 2008).

Figure S2

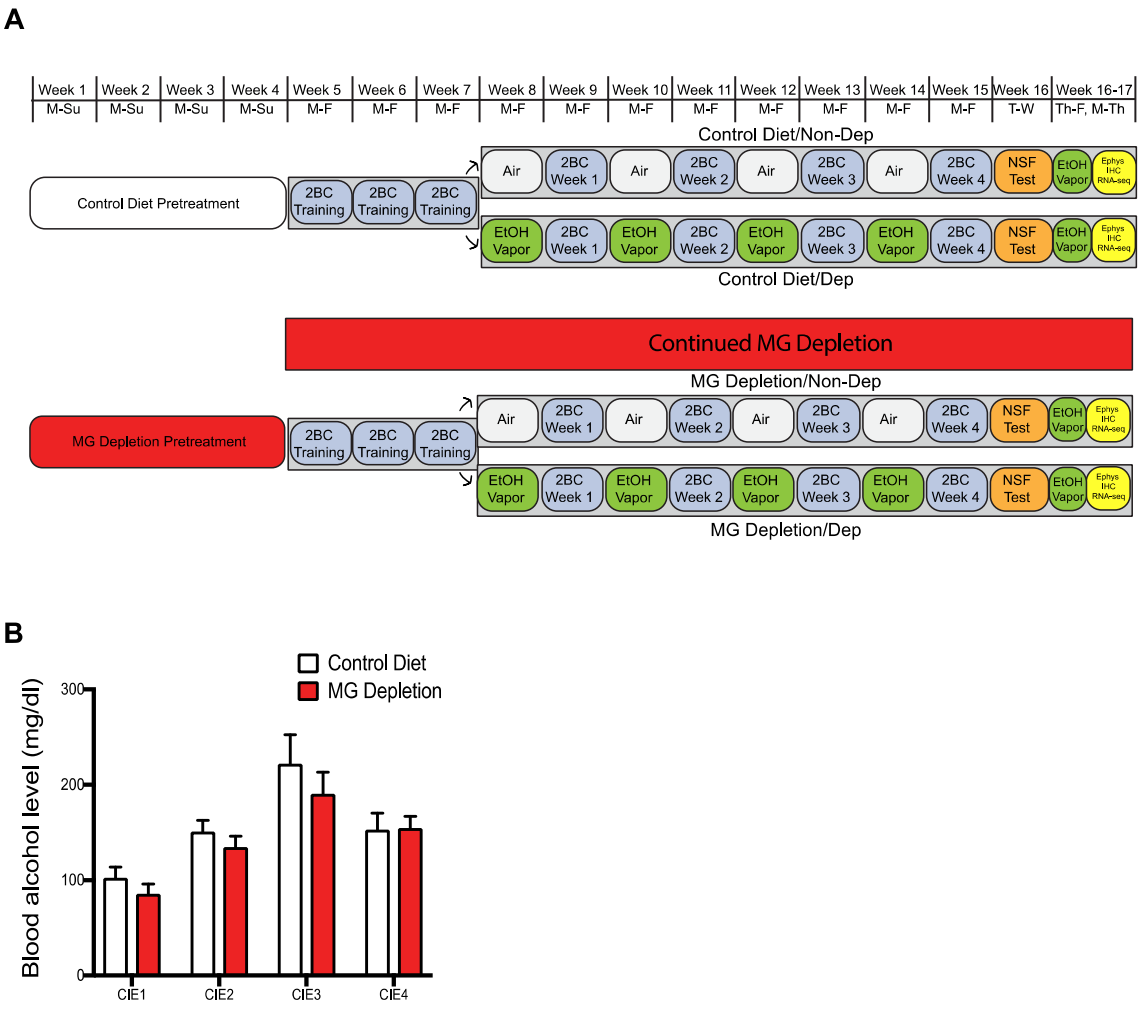

Figure S2. Experimental timeline and blood alcohol levels. (a) Experimental timeline. EtOH=ethanol, 2BC=two bottle choice, NSF=novelty suppressed feeding, IHC=immunohistochemistry, Ephys=electrophysiology. (b) Blood alcohol levels after each week of chronic intermittent ethanol treatment.

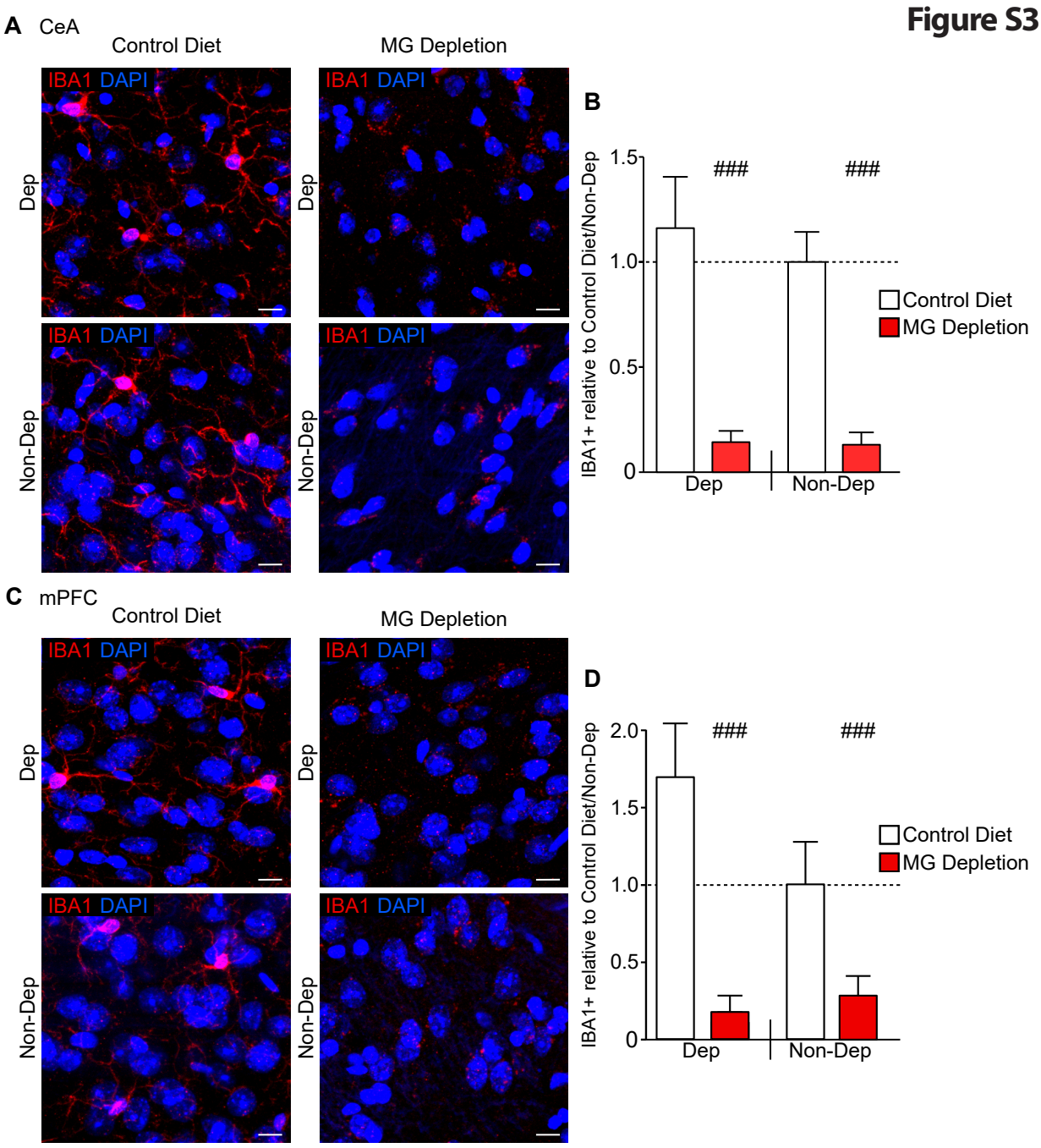

Figure S3. Depletion of the MG marker IBA1 in PLX5622-treated mice. (a) Representative images of the CeA display Ionized Calcium Binding Adaptor Molecule 1 (IBA1) (red) with the nuclear stain DAPI (blue). (b) Graph indicates the change in the percent of cells expressing IBA1 (IBA1+ cells) in the region of interest (ROI) with Dependence (Dep) and/or microglia (MG) Depletion relative to Control Diet/Non-Dependent (Non-Dep) (as indicated by dotted line). MG Depletion decreased IBA1+ in

both Dep and Non-Dep mice, and a significant main effect of diet was observed in the CeA (two-way ANOVA: $F(1, 29)=34.87$, $P=2.07e-6$). Control Diet/Dep, n=10 images; Control Diet/Non-Dep, n=6 images; MG Depletion/Dep, n=9 images; MG Depletion/Non-Dep, n=8 images. (c) Representative images of the mPFC showing IBA1 (red) and DAPI (blue). (d) Graph indicates the change in the percent of cells expressing IBA1+cells in the ROI with Dep and/or MG Depletion relative to Control Diet/Non-Dep in mPFC. MG depletion decreased IBA1+ in both Dep and Non-Dep mice, and a significant main effect of diet was observed in the mPFC (two-way ANOVA: $F(1, 29)=18.17$, $P=0.0002$). Control Diet/Dep, n=10; Control Diet/Non-Dep, n=8; MG Depletion/Dep, n=9; MG Depletion/Non-Dep, n=6. Scale bar = 10μm. Data are presented as mean±SEM values; ### $P<0.001$.

Figure S4

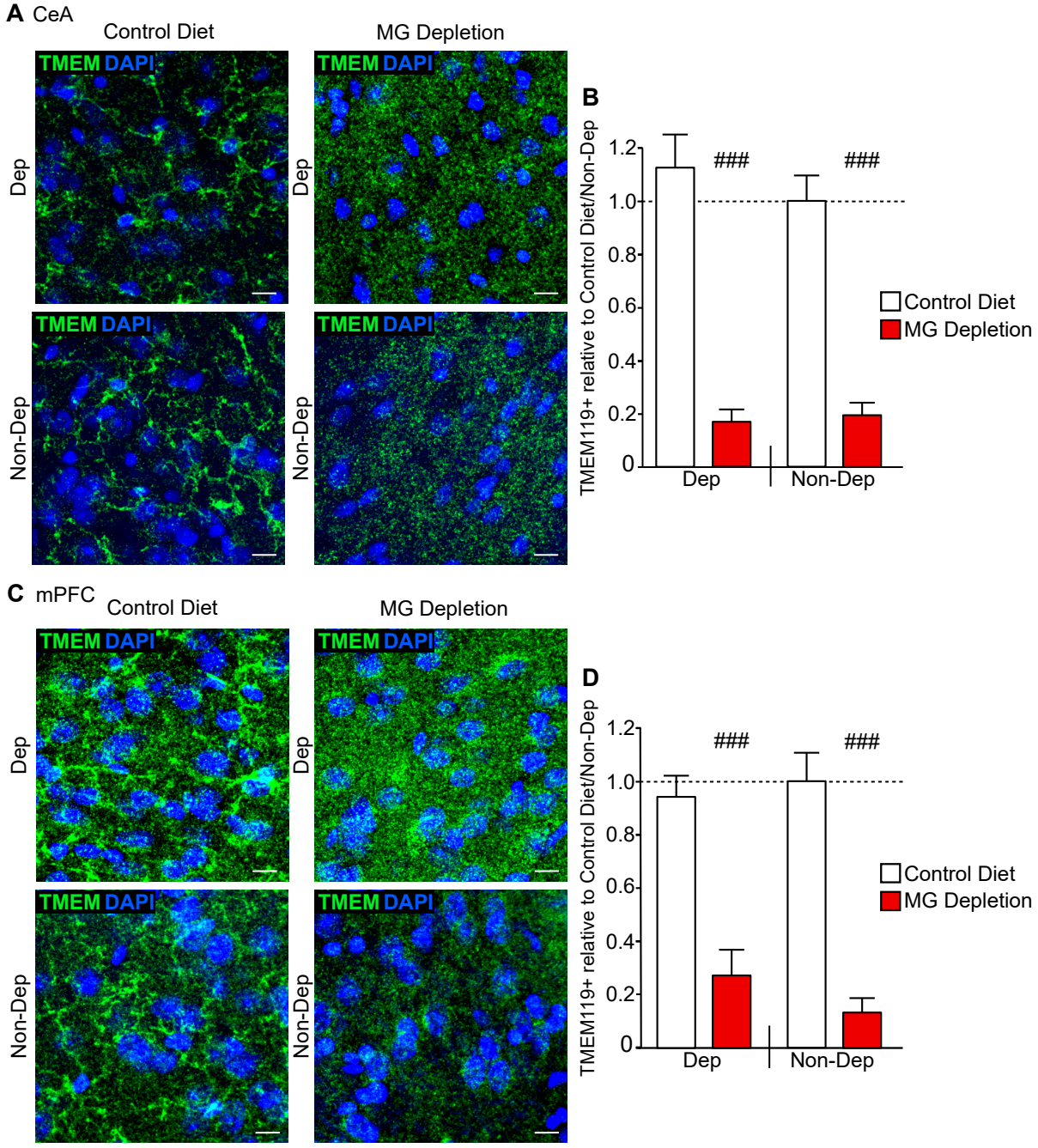

Figure S4. Depletion of the MG marker TMEM119 in PLX5622-treated mice. (a) Representative images of the CeA showing Transmembrane Protein 119 (TMEM119) (green) with the nuclear stain DAPI (blue). (b) Graph indicates the change in the percent of cells expressing TMEM119 (TMEM119+ cells) in the region of interest (ROI) with Dependence (Dep) and/or microglia (MG) Depletion relative to Control Diet/Non-Dependent (Non-Dep) (as indicated by dotted line) in CeA. MG depletion decreased

TMEM119+ in both Dep and Non-Dep mice compared with Control Diet, and a significant main effect of diet was observed in the CeA (two-way ANOVA: $F(1, 29)=98.42$, $P=7.9e-11$). Control Diet/Dep, n=10 images; Control Diet/Non-Dep, n=6 images; MG Depletion/Dep, n=9 images; MG Depletion/Non-Dep, n=8 images. (c) Representative images of the mPFC showing TMEM119 (green) and DAPI (blue) staining. (d) Graph indicates the change in the percent of cells expressing TMEM119+ in the mPFC ROI with Dep and/or MG Depletion relative to Control Diet/Non-Dep in mPFC. MG Depletion decreased TMEM+ in both Dep and Non-Dep mice, and a significant main effect of diet was observed in the mPFC (two-way ANOVA: $F(1, 29)=72.77$, $P=2.13e-9$). Control Diet/Dep, n=10 images; Control Diet/Non-Dep, n=8 images; MG Depletion/Dep, n=9 images; MG Depletion/Non-Dep, n=6 images. Scale bar=10μm. Data are presented as mean±SEM values; ### $P<0.001$.

Figure S5

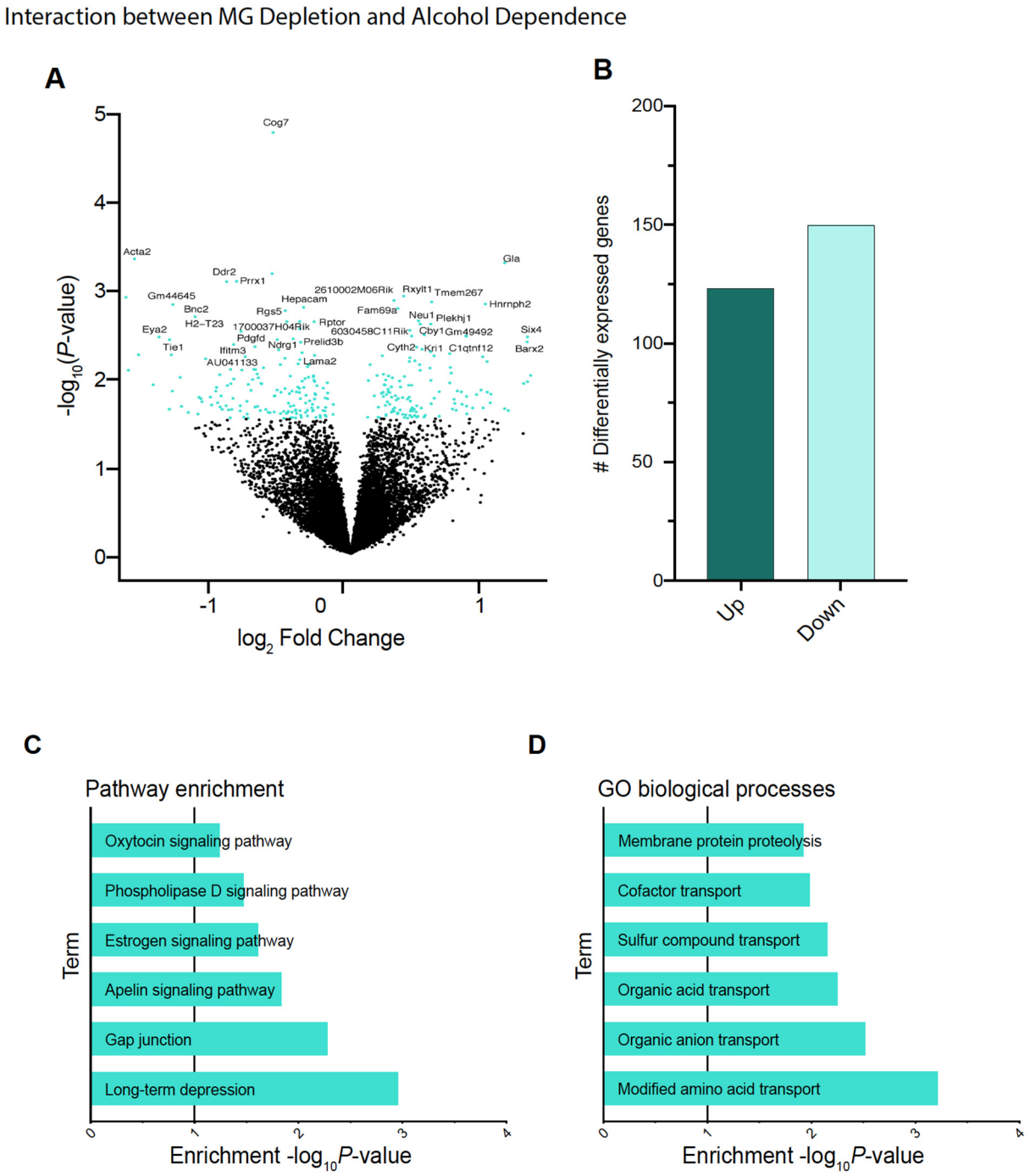

Figure S5. mPFC transcriptome is altered after MG depletion and alcohol dependence. (a) Volcano plot showing $\log_2$ Fold Change against $\log_{10}$ *P*-value for the interaction (two-way ANOVA) between microglia (MG) Depletion and alcohol dependence (Dep). Differentially expressed gene (DEG) ($P<0.05$) are shown as

turquoise dots. The top DEG are labeled. (b) Number of upregulated and downregulated DEG in the mPFC ($P<0.05$) for MG Depletion/Dep compared with MG Depletion/Non-Dep mice. (c, d) Pathway enrichment and gene ontology (GO) biological process analysis for genes identified for the interaction between MG Depletion and alcohol dependence.

Figure S6

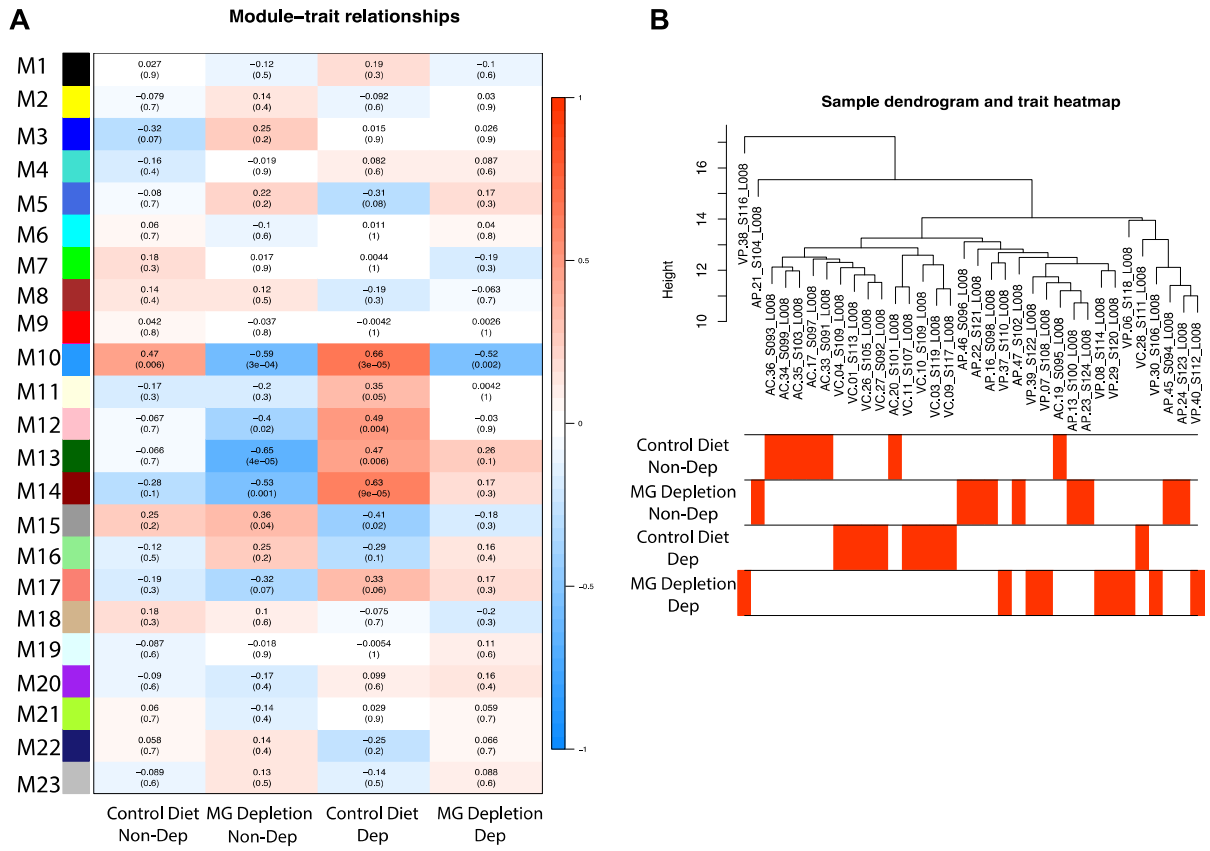

Figure S6. Sample clustering, module detection and correlation between modules, MG depletion treatment and alcohol consumption traits. (a) Heatmap of module-trait relationships for groups with microglia (MG) Depletion and type of alcohol exposure as the trait. *P*-values between detected modules (y-axis) and treatment (x-axis) are shown in the boxes. Color indicates direction of association; red=positive correlation with MG Depletion/Dep (alcohol dependent) and blue=negative correlation with MG Depletion/Dep. (b) Sample dendrogram and trait heatmap were clustered according to differential expression data; no outliers were detected. Red represents MG depletion treatment. Sample traits (rows) are separated by group.

Figure S7

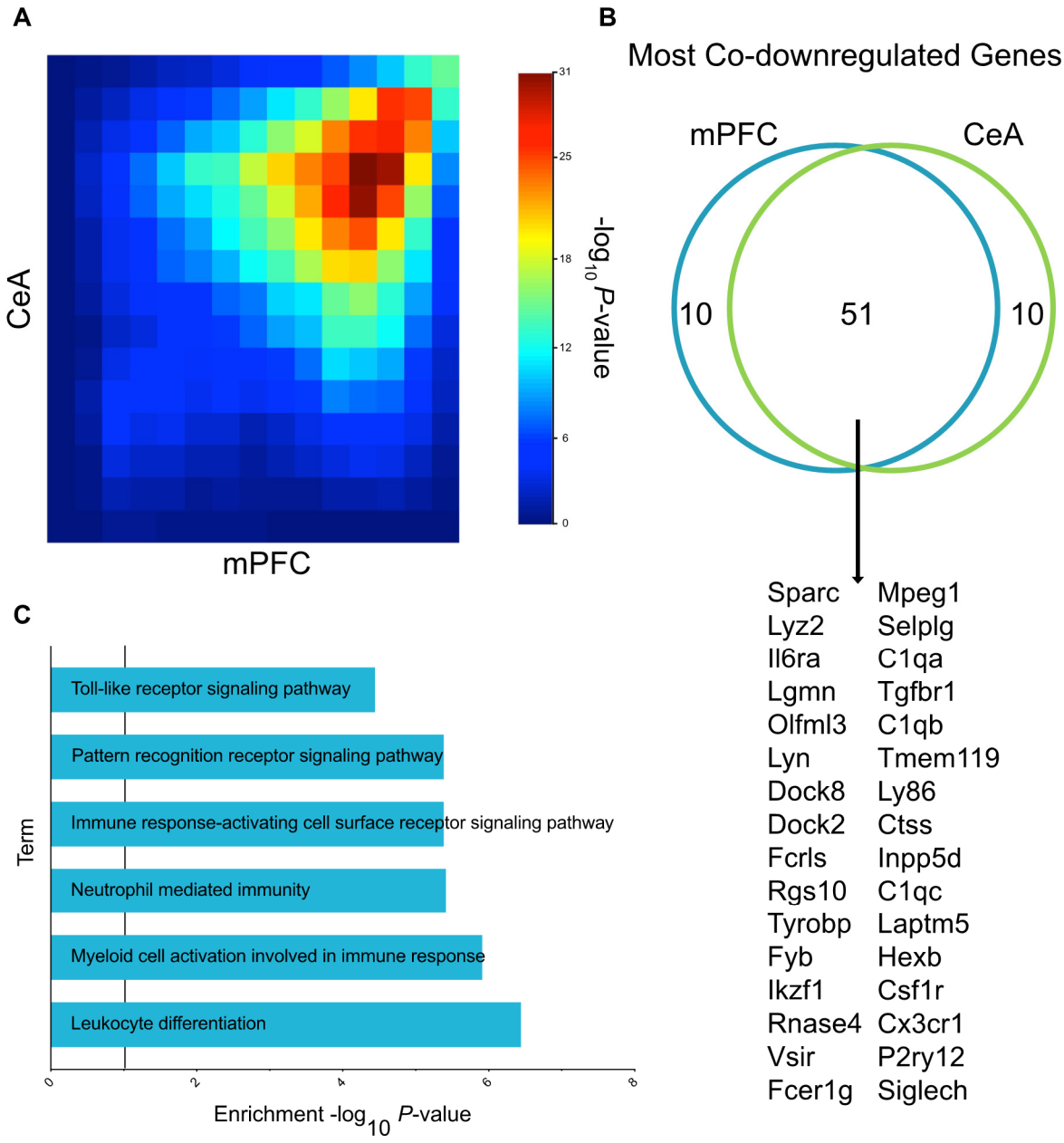

Figure S7. MG depletion gene expression signature is conserved between brain regions. (a) Rank rank hypergeometric overlap map compares threshold-free differential expression between the mPFC and the CeA in microglia (MG) Depletion animals. Each pixel represents the overlap between the MG depletion transcriptome (ANOVA main effect of MG depletion) of the mPFC and CeA with the significance of overlap (-log$_{10}$(*P*-value) of a hypergeometric test; color coded with a step size of 200.

The extent of overlap in the upper right corner represents overlap of co-downregulated genes between brain regions, max $-\log_{10}(P\text{-value})=36$. (b) Venn diagram shows extent of overlap between the most co-downregulated genes in the mPFC and CeA, with a selection of canonical MG markers shown below. (c) Enriched gene ontology terms for the most co-downregulated genes between regions in MG Depletion mice demonstrate a common MG Depletion signature between regions.

Figure S8

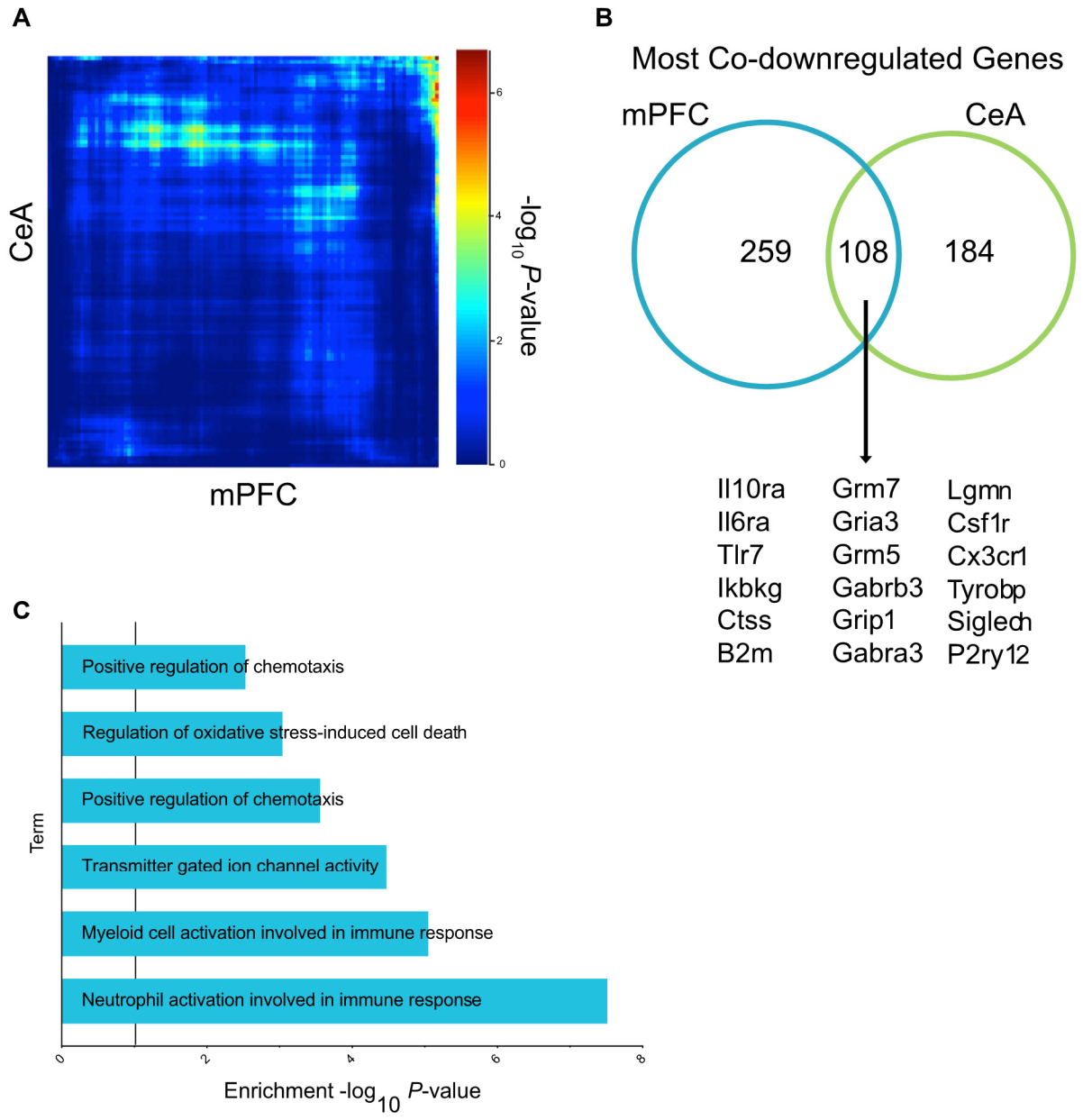

Figure S8. MG depletion co-regulates common gene expression profiles in the mPFC and CeA after alcohol dependence. (a) Rank rank hypergeometric overlap map compares threshold-free differential expression between the mPFC and the CeA in microglia (MG) Depletion animals. Each pixel represents the overlap between the MG Depletion/Dep (alcohol dependent) transcriptome of the mPFC and CeA with the

significance of overlap (-$\log_{10}$(*P*-value) of a hypergeometric test; color coded with a step size of 200). The extent of overlap (shown in the upper right corner) represents overlap of co-downregulated genes between brain regions, max -$\log_{10}$(*P*-value)=6. (b) Venn diagram shows extent of overlap between most co-downregulated genes in the mPFC and CeA, with a selection of immune response genes, synaptic genes and canonical MG markers shown below. (c) Enriched gene ontology terms for the most co-downregulated genes between regions in MG Depletion/Dep animals indicate co-regulation of immune response, MG activation and synaptic function.

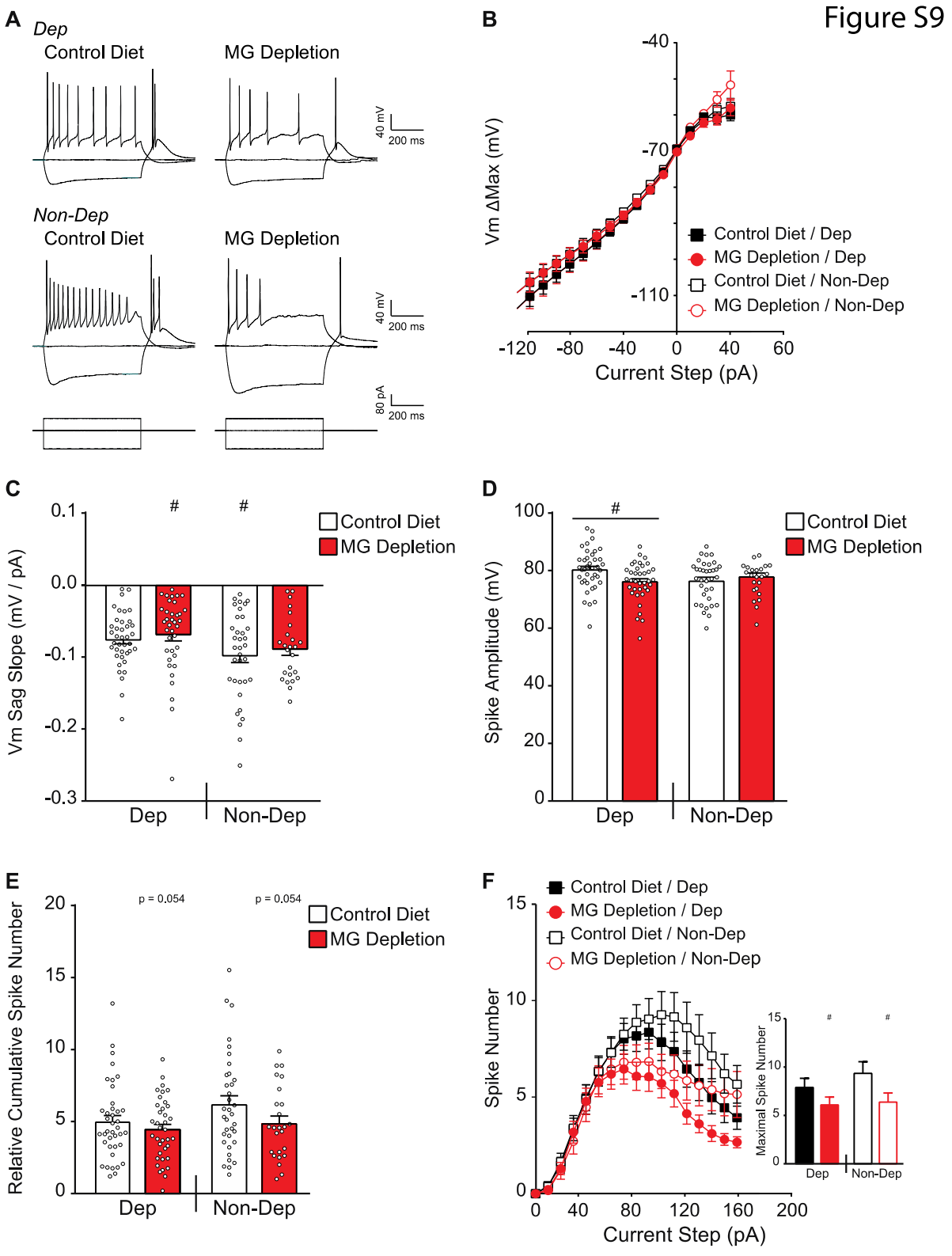

Figure S9. MG depletion alters active membrane properties and excitability of CeA neurons. (a) Representative recordings from CeA neurons from Control Diet or

microglia (MG) Depletion mice that were alcohol dependent (Dep) or non-dependent (Non-Dep). b) voltage/current relationship, (c) voltage sag slope, (d) action potential amplitude, (e) relative cumulative action potential number and (f) action potential number (inset shows maximal number of spikes) are shown. Data are presented as mean±SEM values; # indicates main effect (P<0.05) of diet by two-way ANOVA.

Supplemental Tables

Table S1. A complete list of differentially expressed genes in the mPFC after MG depletion and alcohol dependence. *See Excel file.*

Table S2. A complete list of genes in the mPFC belonging to each module after WGCNA analysis. *See Excel file.*

Table S3. A complete list of differentially expressed genes in the CeA after MG depletion and alcohol dependence. *See Excel file.*

Table S4. Passive membrane properties of CeA neurons. Data are expressed as mean ± SEM, and statistical significance (# main effect of the treatment) $P < 0.05$ was calculated by 2-way ANOVA. *n* indicates the number of cells.

Group	Resistance (MΩ)	Capacitance (pF)	Time Constant (ms)	Voltage Sag Slope (mV/pA)	ADP Slope (mV/pA)	Rheobase (pA)	Spike Threshold (mV)
Control Diet/Dep (n=39)	553.5 ± 36.19	74.47 ± 4.22	27.64 ± 1.29	-0.0746 ± 0.006#	-0.0966 ± 0.0097	24.47 ± 3.21	-46.23 ± 0.66
MG Depletion/Dep (n=37)	557.5 ± 42.85	77.97 ± 4.87	26.52 ± 1.36	-0.0625 ± 0.0071#	-0.0742 ± 0.0092	25.03 ± 2.77	-44.47 ± 0.75
Control Diet/Non-Dep (n=35)	548.6 ± 39.78	72.85 ± 4.53	27.10 ± 1.37	-0.0966 ± 0.0103	-0.1110 ± 0.0167	28.00 ± 3.583	-44.97 ± 0.73
MG Depletion/Non-Dep (n=25)	572.6 ± 42.38	73.71 ± 4.38	28.73 ± 1.29	-0.0882 ± 0.0088	-0.1076 ± 0.0124	25.74 ± 3.12	-44.30 ± 1.05

Table S5. Action potential properties of CeA neurons. The data are presented as mean ± SEM, and statistical significance, marked as # main effect of the treatment, and * compared to Control Diet/Dep, P <0.05 was calculated by 2-way ANOVA and Sidak post hoc test. *n* indicates the number of cells.

Group	Amplitude (mV)	Half-Width (ms)	After-hyperpolarization (mV)	Maximal Positive Slope (mV/ms)	Maximal Negative Slope (mV/ms)	Pos/Neg Slope Ratio
Control Diet/Dep (n=39)	80.52 ± 1.14	1.52 ± 0.041	9.07 ± 0.73	153.6 ± 6.97	-53.33 ± 1.99	2.81 ± 0.083
MG Depletion/Dep (n=37)	76.05 ± 1.11*	1.57 ± 0.048$^{\#}$	9.72 ± 0.88	143.3 ± 5.48	-49.53 ± 1.93	2.86 ±0.097
Control Diet/Non-Dep (n=35)	76.62± 1.20	1.43 ± 0.041	10.97 ± 0.91	149.1 ± 6.60	-52.89 ± 1.64	2.62 ± 0.090
MG Depletion/Non-Dep (n=25)	77.76± 1.32	1.61 ± 0.061$^{\#}$	10.90 ± 1.07	142.8 ± 8.53	-50.34 ±2.53	2.807 ± 0.177

Supplemental References

1. Bajo M, Montgomery SE, Cates LN, Nadav T, Delucchi AM, Cheng K, et al. (2016): Evaluation of TLR4 Inhibitor, T5342126, in Modulation of Ethanol-Drinking Behavior in Alcohol-Dependent Mice. *Alcohol Alcohol*. 51:541-548.

2. Huitron-Resendiz S, Nadav T, Krause S, Cates-Gatto C, Polis I, Roberts AJ (2018): Effects of Withdrawal from Chronic Intermittent Ethanol Exposure on Sleep Characteristics of Female and Male Mice. *Alcohol Clin Exp Res*. 42:540-550.

3. Becker HC, Lopez MF (2004): Increased ethanol drinking after repeated chronic ethanol exposure and withdrawal experience in C57BL/6 mice. *Alcohol Clin Exp Res*. 28:1829-1838.

4. del Rey A, Balschun D, Wetzel W, Randolf A, Besedovsky HO (2013): A cytokine network involving brain-borne IL-1beta, IL-1ra, IL-18, IL-6, and TNFalpha operates during long-term potentiation and learning. *Brain Behav Immun*. 33:15-23.

5. Bennett ML, Bennett FC, Liddelow SA, Ajami B, Zamanian JL, Fernhoff NB, et al. (2016): New tools for studying microglia in the mouse and human CNS. *Proc Natl Acad Sci U S A*. 113:E1738-1746.

6. Rosenzweig N, Dvir-Szternfeld R, Tsitsou-Kampeli A, Keren-Shaul H, Ben-Yehuda H, Weill-Raynal P, et al. (2019): PD-1/PD-L1 checkpoint blockade harnesses monocyte-derived macrophages to combat cognitive impairment in a tauopathy mouse model. *Nat Commun*. 10:465.

7. Suchorukova EG, Kirik OV, Korzhevskii DE (2010): The use of immunohistochemical method for detection of brain microglia in paraffin sections. *Bull Exp Biol Med*. 149:768-770.

8. Schindelin J, Arganda-Carreras I, Frise E, Kaynig V, Longair M, Pietzsch T, et al. (2012): Fiji: an open-source platform for biological-image analysis. *Nat Methods*. 9:676-682.

9. R Core Team (2018): R: A language and environment for statistical computing. *Foundation for Statistical Computing, Vienna, Austria*.

10. Lohman BK, Weber, J.N., Bolnick, D.I. (2016): Evaluation of TagSeq, a reliable low-cost alternative for RNAseq. *Molecular Ecology Resources*. 16:1315-1321.

11. Munro SA, Lund SP, Pine PS, Binder H, Clevert DA, Conesa A, et al. (2014): Assessing technical performance in differential gene expression experiments with external spike-in RNA control ratio mixtures. *Nat Commun*. 5:5125.

12. Zhang B, Horvath S (2005): A general framework for weighted gene co-expression network analysis. *Stat Appl Genet Mol Biol*. 4:Article17.

13. McCarthy GM, Farris SP, Blednov YA, Harris RA, Mayfield RD (2018): Microglial-specific transcriptome changes following chronic alcohol consumption. *Neuropharmacology*. 128:416-424.

14. Wang J, Vasaikar S, Shi Z, Greer M, Zhang B (2017): WebGestalt 2017: a more comprehensive, powerful, flexible and interactive gene set enrichment analysis toolkit. *Nucleic Acids Res*. 45:W130-W137.

15. Chen EY, Tan CM, Kou Y, Duan Q, Wang Z, Meirelles GV, et al. (2013): Enrichr: interactive and collaborative HTML5 gene list enrichment analysis tool. *BMC Bioinformatics*. 14:128.

16. Shannon P, Markiel A, Ozier O, Baliga NS, Wang JT, Ramage D, et al. (2003): Cytoscape: a software environment for integrated models of biomolecular interaction networks. *Genome Res*. 13:2498-2504.

17. Zhang Y, Chen K, Sloan SA, Bennett ML, Scholze AR, O'Keeffe S, et al. (2014): An RNA-sequencing transcriptome and splicing database of glia, neurons, and vascular cells of the cerebral cortex. *J Neurosci*. 34:11929-11947.

18. Plaisier SB, Taschereau R, Wong JA, Graeber TG (2010): Rank-rank hypergeometric overlap: identification of statistically significant overlap between gene-expression signatures. *Nucleic Acids Res*. 38:e169.

19. Cahill KM, Huo Z, Tseng GC, Logan RW, Seney ML (2018): Improved identification of concordant and discordant gene expression signatures using an updated rank-rank hypergeometric overlap approach. *Sci Rep*. 8:9588.

20. Bagot RC, Cates HM, Purushothaman I, Lorsch ZS, Walker DM, Wang J, et al. (2016): Circuit-wide Transcriptional Profiling Reveals Brain Region-Specific Gene Networks Regulating Depression Susceptibility. *Neuron*. 90:969-983.

21. Patel RR, Khom S, Steinman MQ, Varodayan FP, Kiosses WB, Hedges DM, et al. (2019): IL-1beta expression is increased and regulates GABA transmission following chronic ethanol in mouse central amygdala. *Brain Behav Immun*. 75:208-219.

22. Roberts AJ, Khom S, Bajo M, Vlkolinsky R, Polis I, Cates-Gatto C, et al. (2019): Increased IL-6 expression in astrocytes is associated with emotionality, alterations in central amygdala GABAergic transmission, and excitability during alcohol withdrawal. *Brain Behav Immun*. 82:188-202.